ARTICLE

Porous graphene/poly(vinylidene fluoride) nanofibers for pressure sensing

Mohammad Mahdi Abolhasani[1,2] | Sara Azimi[1,2] | Masoud Mousavi[2] |
Saleem Anwar[1] | Morteza Hassanpour Amiri[1] | Kamyar Shirvanimoghaddam[3] |
Minoo Naebe[3] | Jasper Michels[1] | Kamal Asadi[1,4,5]

[1]Max-Planck Institute for Polymer Research, Mainz, Germany

[2]Chemical Engineering Department, University of Kashan, Kashan, Iran

[3]Carbon Nexus, Institute for Frontier Materials, Deakin University, Geelong, Australia

[4]Department of Physics, University of Bath, Bath, UK

[5]Centre for Therapeutic Innovations, University of Bath, Bath, UK

Correspondence
Mohammad Mahdi Abolhasani and Kamal Asadi, Max-Planck Institute for Polymer Research, Ackermannweg 10, 55128, Mainz, Germany.
Email: abolhasani@kashanu.ac.ir (M. M. A.) and ka787@bath.ac.uk (K. A.)

Abstract

Piezoelectric polymers have emerged as promising materials for application in pressure sensing devices in particular for wearable applications, where inorganic piezoelectric materials can face limitations due to their brittleness. One of the bottlenecks for the adaptation of piezoelectric polymers is their relatively weak piezoelectric voltage coefficient. Hence there have been numerous efforts to improve the performance of the comprising devices by making composites of poly(vinylidene fluoride) (PVDF), or through making porous PVDF films, or by nanostructuring. Here, we demonstrate the fabrication of porous nanofibers with graphene/PVDF composites and investigate the suitability of the fiber for motion sensing. The nanofibers are fabricated by electrospinning from the solution phase. Guided by an experimentally validated phase diagram for PVDF/solvent/non-solvent ternary system, porous graphene/PVDF nanofibers with different porosities and pore morphologies have been produced through solidifying the fibers in the binodal or spinodal regions of the phase diagram. It is found that only by solidifying the composite fibers in the spinodal region, graphene loading of 0.1 wt% promotes the formation of the electroactive phase substantially, and the resulting fibers exhibit enhanced piezoelectric output. It is further shown that the comprising sensors are biocompatible and show high sensitivity to body motion.

KEYWORDS
applications, differential scanning calorimetry, electrospinning, fibers

1 | INTRODUCTION

The development of wearable piezoelectric sensors for motion monitoring has received a great deal of attention over the last decade.[1] Piezoelectric materials convert mechanical vibrations into electrical signals,[2–4] which can be detected and processed by a peripheral circuit, thereby enabling the development of motion sensors. The important material parameter is the piezoelectric voltage coefficient, g_{33}, which is defined as $g_{33} = d_{33}/\varepsilon_{33}$, where

d_{33} is piezoelectric charge coefficient, and ε_{33} is the relative permittivity of the material. The electrical signal, or open circuit voltage, V_{OC}, that is generated by the piezoelectric under mechanical action is obtained from the following relationship $V_{OC} = g_{33}.d.F/A$, where d and A are the thickness and area of the device, and F is the applied mechanical force. Evidently, large V_{OC} values would enable the fabrication of sensitive sensors.

Ceramic-based piezoelectric materials such as $PdZrTiO_3$ (PZT) and $BaTiO_3$ (BTO)[5-7] are inherently brittle, which makes their application in wearable sensors challenging because the sensors can go through extreme bending or twisting cycles. Furthermore, PZT is subject to health regulation as it contains lead.[8]

Poly(vinylidene fluoride) PVDF, and its copolymers are highly attractive alternative materials for the fabrication of flexible and biocompatible piezoelectric sensors. Despite a substantially lower d_{33} value of ~ -30 pV/m, PVDF exhibits a g_{33} that is comparable to inorganic piezoelectric materials. Interestingly, the g_{33} value can be further enhanced through film engineering, and by making porous PVDF films. One challenge; however, is to create the electroactive phase in PVDF, because PVDF is known to have five crystalline phases. Crystallization of PVDF in its non-piezoelectric α-phase is usually favored, which is the most thermodynamically stable one. Biaxial stretching is usually required to convert the α-phase into the piezoelectric β-phase. It has been shown that electrospinning of PVDF alleviates the need for mechanical stretching and produces PVDF nanofibers that are readily crystallized in the β-phase.[9-12]

PVDF fibers are promising structures for various applications such as sensors[13,14] and fabrication of carbon fibers, which are useful for energy storage devices.[15] Electrospun PVDF fibers have been converted into carbon fiber using a low-temperature chemical stabilization treatment and carbonization.[15] Piezoelectric PVDF fibers-based sensors have been employed in various applications to detect human motion,[16,17] achieve ultra-sensitive pressure sensors,[18-20] or to localize impact with strain sensor.[21,22] Interestingly, devices fabricated from PVDF nanofibers have shown higher instantaneous electrical output signals in comparison with the pristine PVDF film.[9,10] Hence, there is an intensified research effort to further enhance the electrical output signals from PVDF nanofibers to improve the performance of the comprising pressure sensors.[23] An increase in piezo-response has been reported for nanofibers made of PVDF composite with a nanofiller such as cellulose nanocrystals (CNC), carbon nanotubes (CNT), and nanoparticles of Ag, ZnO, LiCl, $NaNbO_3$, polyaniline, and hybrid fillers.[24-27] It has been shown that decorated multiwall CNT or core-shell

nanoparticles can increase the output voltage of PVDF fibers.[28,29] Among various materials, graphene-based fillers have shown a promising prospect in enhancing the voltage response of the composite fibers fabricated thereof.[18,30]

An alternative approach to increase the voltage response in nanofibers is to create porous nanofibers.[31] The increased voltage response, under the same mechanical forces, is ascribed to the reduced effective permittivity of the composite, which consequently leads to an increase in the piezoelectric voltage constant of the fibers.[31-35] It has been shown that the pore structure, that is, closed versus open pore, and the amount of porosity, are the key parameters that affect the voltage response.[36]

Incorporating porosity[35,37] and nanofillers, in particular graphene-based materials,[10] have independently been successful in increasing the voltage response of PVDF-based systems. A question that arises is that whether simultaneous incorporation of nanofillers and porosity in PVDF nanofiber would yield a higher voltage response. However, to the best of our knowledge, both techniques have never been attempted at the same time. It is therefore not clear whether a synergistic interaction can be created and a larger voltage response could be achieved. Here, for the first time, it is shown that porous nanofibers of graphene/PVDF composites can be readily obtained by engineering the polymer solution and that through optimizing the composition, a voltage response can be obtained that is larger than the response of only graphene/PVDF or porous nanofibers. The porosity is created by introducing water as non-solvent. Control over the porosity is achieved by establishing the thermodynamics of the PVDF/solvent/non-solvent mixture[38] through a careful choice of composition. Incorporation of water in the polymer solution leads to liquid–liquid phase separation of an otherwise homogeneous polymer solution. The polymer solution separates into two coexisting solvent-rich and PVDF-rich liquid phases, where the solvent-rich phase turns into pores that are randomly distributed through the volume of the fiber. We show that the voltage response of the porous graphene/PVDF nanofibers depends on whether the solution is solidified in the binodal or spinodal parts of the ternary phase diagram, with the former producing fibers with a large voltage response. Furthermore, it is shown that the resulting porous composite graphene/PVDF nanofiber is biocompatible. Finally, the nanofibers are employed in sensors that enable detection of body movements such as walking, or gentle body movements, such as wrist and elbow bending. These findings imply that the porous graphene/PVDF sensors can be suited for application in human motion monitoring devices.

2 | EXPERIMENTAL

PVDF (Mw = 275,000 g/mole, Mn = 107,000 g/mole) and N, N-dimethylformamide (DMF), poly(vinyl alcohol) PVA were purchased from Sigma Aldrich. Graphene nanoplatelets were supplied from XG Science Inc. All materials were used as received.

To determine the cloud points, PVDF solutions in DMF with various concentrations ranging from 1 to 20 wt% were prepared. Then, at a constant stirring temperature of 20°C, water was added dropwise to the solution until the initially homogeneous and clear solution turned turbid. The turbidity concentrations were recorded as cloud points.

Porous and non-porous graphene/PVDF nanofibers were prepared using the compositions presented in Table 1. A reference sample (K0) without water and graphene was also prepared. For the porous sample, two series of samples were prepared, with different water concentrations of 2.5%wt (B-samples) and 4%wt (S-samples). All the solutions were sonicated for 20 min followed by stirring at 70°C overnight. To electrospun the fibers, voltage, working distance and feeding rate of 20 kV, 17 cm, and 1 ml/h were used, respectively. The electrospinning parameters were the same for all samples.

To analyze the morphology of the nanofibers, scanning electron microscopy (SEM) (Zeiss Supra 55VP) was used. The SEM images were analyzed using ImageJ to obtain the mean diameter of the nanofibers. To reveal the porous microstructure, nanofibers were immersed in a 10 wt% PVA water solution overnight. After a drying step in an oven at 75°C for 24 h, the nanofibers were broken in liquid nitrogen. The cross-section was imaged by SEM after removal of PVA.

Fourier transfer infrared (FTIR) spectroscopy was performed to analyze polymorphism and the crystalline structure of the nanofibers, respectively. FTIR Bruker 70 spectra were recorded from 600 to 1600 cm^{-1} with a resolution of 4 cm^{-1}. Differential scanning calorimetry (DSC [TA Instrument Q200]) was conducted by heating the nanofibers from room temperature to 220°C with a heating rate of 10°C/min.

To test biocompatibility of the nanofibers, mouse embryonic fibroblasts (MEF) were cultured with DMEM medium (1×), supplemented with 10% fetal bovine serum (Gibco) and 1% penicillin–streptomycin solution in a 75 cm^2 flask which was placed in a humidified atmosphere with 5% CO_2 at 37°C. The cultured cells were seeded in a 96-well plate on the designed pressure sensor after 3 days. Then, MEF cells viability was evaluated using the MTT (3-[4,5-dimethyldiazol-2-yl]-2,5-diphenyl tetrazolium bromide) assay. The analytical assay was performed after 1, 2, and 3 days. Moreover, immunofluorescence staining was performed with graphene/PVDF nanofibers. To that end, DAPI was used to stain the nucleus of MEF cells. First, the sample was fixed with paraformaldehyde 4% for 20 min and then rinsed three times with prewarmed PBS (1×). At the final step, the samples were incubated for 5 min at room temperature with DAPI. An inversion fluorescence microscope was employed to observe the morphology of the cells.

To characterize the voltage response of the sensors, a mat of the nanofibers (20 × 20 × 0.05 mm^3) was sandwiched between two aluminum electrodes. The sensors were then impacted using a custom-built cyclic impacting device at the frequency of 1 Hz with impact pressure of 0.2 MPa. Finally, a Tektronix oscilloscope was used to record the voltage response, V_{OC}, of the fibers.

TABLE 1 Composition of different graphene/PVDF solutions

Sample code	Water (~vol%)	PVDF (~vol%)	DMF (~vol%)	Graphene (wt%)
K0(Ref)	0	10	89	0
G0.1	0	10	89	0.1
G1	0	10	89	1
G3	0	10	89	3
B0	3.4	10	89	0
B0.1	3.4	10	89	0.1
B1	3.4	10	89	1
B3	3.4	10	89	3
S0	5.4	10	89	0
S0.1	5.4	10	89	0.1
S1	5.4	10	89	1
S3	5.4	10	89	3

Abbreviations: DMF, dimethylformamide; PVDF, poly(vinylidene fluoride).

3 | RESULTS AND DISCUSSION

To obtain porous structure within PVDF electrospun fibers, it is essential to gain more insight into the thermodynamic as well as the kinetics of phase separation of the ternary PVDF/DMF/water phase diagram. Calculation of the ternary phase diagram is conducted based on the Flory-Huggins (FH) Gibbs free energy of mixing (ΔG_M)[39] for the ternary system following Equation (1):

$$\frac{\Delta G_M}{RT} = n_1 ln\varphi_1 + n_2 ln\varphi_2 + n_3 ln\varphi_3 + n_1\varphi_2 g_{12}(u_2) + n_2\varphi_3 + n_1\varphi_3\chi_{13},$$

(1)

where n_i and ϕ_i are the number of moles and the volume fraction of component i, respectively; R and T denote the universal gas constant (8.314 J/mol.K) and the absolute temperature (K), respectively. χ_{13} and χ_{23} are water/ PVDF and DMF/PVDF interaction parameters which are assumed to be 2.09 and 0.43,[40] respectively. Finally, $g_{12}(u_2)$ is water / DMF interaction parameter, which can be calculated using:

$$g_{12}(u_2) = \alpha + \frac{\beta}{1 - \gamma u_2},$$

(2)

where $u_2 = \phi_2/(\phi_1 + \phi_2)$ is pseudo-binary mixture and α, β, and γ are considered to be 0.322, 0.075, and 0.960,[41] respectively. The binodal and spinodal curves have been calculated following the method by Altena et al.[42]

The calculated binodal curve is verified using the experimentally determined cloud points, as shown in Figure 1. The fact that the calculated binodal curve fits the experimental data very well reflects the suitability of

Flory-Huggins theory to describe the phase behavior of the PVDF/DMF/water ternary mixture. There are two pathways to create pores, that is, by driving the liquid–liquid phase separation through the binodal or spinodal regions of the phase diagram during the electrospinning and drying stage of the nanofibers. Therefore, the composition of the spinning dopes is designed such that the phase separation in the PVDF/DMF/water ternary mixture is passed through the binodal (the B-series) or spinodal (the S-series) regions of the phase diagram.[35] For every series, various amounts of graphene fillers are added.

Guided by the theory, various amounts of graphene are now added to the solutions. Representative SEM images of the K0, G0.1, B0.1, and S0 nanofibers and their corresponding cross-sections and diameter distribution are shown in Figure 2. The SEM images of all other nanofibers are presented in the SI (Figures S1 and S2). The insets in Figure 2 clearly show that all fibers have a smooth surface. A solid non-porous core is achieved for the K0 and G0.1 samples, while a porous cross-section is observed for B0.1 and S0, following theoretical predictions. The porous structure is formed because in these samples the thermodynamically unstable polymer solution is separated into two liquid phases, that is, solvent-rich phase and polymer-rich phase,[43,44] wherein the interior porosity in the nanofibers is due to the evaporation of the solvent-rich phase. Due to the small amount of water inside the dopes only closed-shell pores are obtained.

Figure S3 shows the change in diameter of the nanofibers with graphene and water content. The diameter of the pristine PVDF nanofibers amounts to 76 ± 32 nm. The G and B samples show almost no change in diameter upon the addition of graphene nanofillers
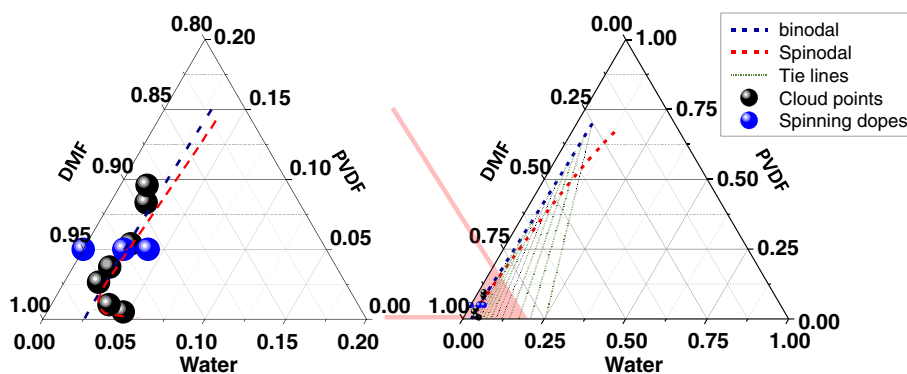
FIGURE 1 Ternary phase diagram of PVDF/DMF/water (right), obtained by fitting a calculated binodal curve (dashed-blue) to experimental cloud point data (black symbols), using Flory-Huggins theory. The calculated spinodal is given by the red dashed line. The blue symbols indicate the composition of the spinning dopes. 0–0.03 gr graphene is added to each dope according to Table 1. A zoom-in of the highlighted region on the phase diagram is given on the left. DMF, dimethylformamide; PVDF, poly(vinylidene fluoride) [Color figure can be viewed at wileyonlinelibrary.com]
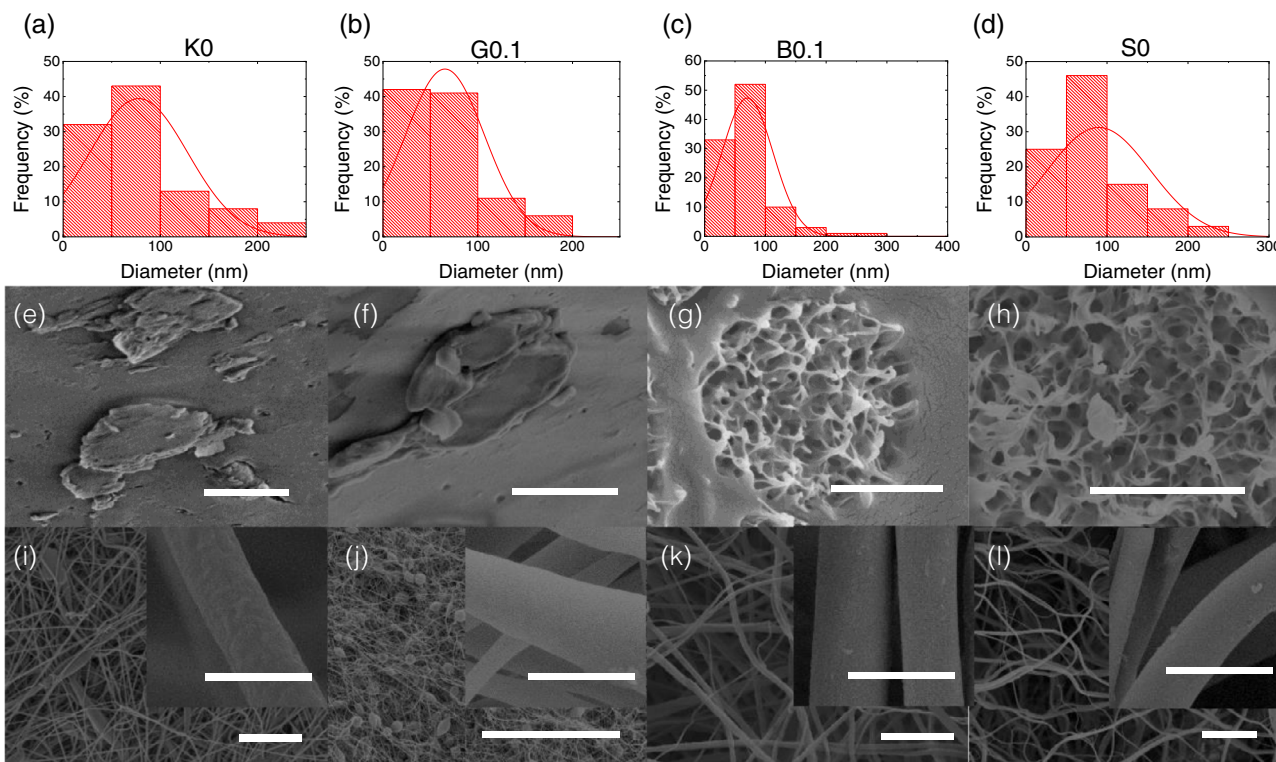
FIGURE 2 (a–d) Representative histograms of PVDF nanofiber diameter for K0, G0.1, B0.1, and S0, with their respective (e–h) cross-sectional SEM images of the nanofibers. The respective random networks of the nanofibers are presented in ref. 10 with the insets showing the surface of each nanofiber. The scale bars are 300 nm, 1 μm, and 100 nm for the cross-section, fibers and inset images, respectively. PVDF, poly(vinylidene fluoride); SEM, scanning electron microscopy [Color figure can be viewed at wileyonlinelibrary.com]

whereas the "S-series" samples have a larger diameter. A small rise in nanofiber diameter upon increasing the graphene content is related to the enhanced viscosity of the dopes.

In the next step, we have determined the crystallinity of all PVDF nanofibers by DSC, FTIR, and XRD analyses. The FTIR and XRD spectra as well as first heating DSC thermograms of the samples are shown in Figures S4, S5, and S6, respectively. The FTIR spectra, Figure S4 shows that all nanofibers have characteristic peaks of both non-piezoelectric α- and piezoelectric β-phases, which appear at 763 and 840 cm^{-1}, respectively.[45] However, the spectra clearly show the absence of the strong α characteristic peak and demonstrate the dominance of the β-phase in the nanofibers. It has been reported that the elongation of the jet during the electrospinning promotes the conversion of the non-piezoelectric α phase into the piezoelectric β-phase.[46,47] We note that all FTIR spectra are normalized to the absorbance peak at 877 cm^{-1}.[48] The fraction of the piezoelectric β-phase, $F(\beta)$, in every samples is quantified using Equation (3)

$$F(\beta) = \frac{A_\alpha}{1.26 A_\alpha + A_\beta},\qquad(3)$$
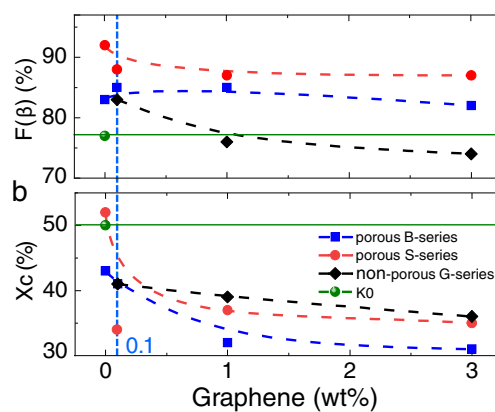
FIGURE 3 (a) β-phase fraction, $F(\beta)$, and (b) crystallinity, X_C versus graphene content for porous and non-porous PVDF/graphene nanofibers. The green lines represent the K0 pristine PVDF nanofiber sample. All lines are drawn as a guide to the eyes. PVDF, poly(vinylidene fluoride) [Color figure can be viewed at wileyonlinelibrary.com]

where A_α and A_β represent the absorption bands at 763 and 840 cm^{-1}, respectively. The plot of $F(\beta)$ versus graphene weight fraction in the PVDF, nanofibers are presented in Figure 3a. In K0 pristine PVDF nanofiber

$F(\beta)$ amounts to 77%. By the addition of 0.1 wt% graphene in the G0.1 sample $F(\beta)$ increases to 84%, but adding more graphene lowers $F(\beta)$ substantially. The crystallization of β-phase can be related to specific interaction between PVDF chains and graphene.[49] However, the β-phase content decreases at higher filler contents due to probable agglomeration of graphene, which leads to decreased chain confinement.[50] In case of porous fibers, B0 and S0 samples have shown higher $F(\beta)$ compared to pristine PVDF fiber. It is speculated that porosity increases the β-phase content which can be due to trapped chains in the confined area between pores.[51] In the B samples, the addition of graphene does not change $F(\beta)$, whereas for the S samples addition of graphene reduces $F(\beta)$ significantly.

To further evaluate the presence of crystal polymorphs in the samples, XRD analysis has been conducted. Figure S5 reveal the presence of three characteristic peaks at $2\theta = 18.5°$, $20.1°$, and $27.0°$ for PVDF-based fibers, which can be assigned to α (020), β ([200], [110]), and α (111) polymorphs, respectively.[11,48,52] Hence, the samples are composed of only α- and β-phases.

DSC thermograms of the samples, Figure S6 illustrate an endothermic peak around 170°C due to the melting of PVDF.[30] Following the determination of the β-phase fraction, the crystallinity of the nanofibers is determined. To that end, the degree of crystallinity, X_C, for each sample is determined using Equation (4):

$$X_C = \frac{\Delta H}{\Delta H_\alpha F(\alpha) + \Delta H_\beta F(\beta)}, \tag{4}$$

where ΔH is the melting enthalpy of the sample; ΔH_α (93.07 Jg^{-1}) and ΔH_β (103.4 Jg^{-1}) are the melting enthalpies of a 100% crystalline sample in the α and β-phase, respectively. The $F(\alpha)$ and $F(\beta)$ are the α and β-phase fractions.

The crystallinity of the G, B, and S nanofiber series are plotted in Figure 3b. The crystalline fraction of the reference PVDF fiber, K0, is 50%. For the G, B, and S samples, crystallinity decreases upon the addition of graphene. Previous studies have suggested that fillers act as nucleating agents and retard the crystallization of PVDF. A larger number of nucleation sites and the formation of small crystals with many defects reduce the crystallinity of both porous and non-porous graphene/PVDF composite nanofibers.[53] The only exception is the S0 sample, wherein X_C is larger than that of the pristine K0 sample. This is in part due to substantially enhanced $F(\beta)$ fraction in this sample.

Samples with increased crystallinity and $F(\beta)$ are suited for sensing applications also for integration in wearable devices. Hence, the fibers should be biocompatible to allow integration of the pressure sensors on the human body. To that end, a mat of fibers with a size of 6×5 cm^2 has been sandwiched in between two flexible electrodes made of Kapton tapes coated with aluminum. The biosafety of the device has been evaluated through in vitro biocompatibility tests. The adherence, growth, and viability of MEF cells on the designed sensors and cell culture dish (the control) have been investigated by both fluorescence microscopy and MTT assays. It is observed, as presented in Figure 4a, that MEF cells adhere to all samples with detectable cell nucleus. The nuclei are round, complete, and not fractionated. Microscopy also reveals that in the nucleus study using DAPI method, the nuclei are not apoptotic and dye has no adverse effect on the MEFs nuclei. The results of the MTT test also shows that 97% viability of the cells after 3 days of culture which proves good biocompatibility of the designed pressure sensor (Figure 4b).

To characterize the voltage response of the sensor, a small flat-head plastic hammer is used to exert a mechanical impact (0.2 MPa) on the electrospun nanofibers. The generated V_{OC} (measured at optimum load resistance of 1 MΩ) at an impact frequency of 1 Hz is shown in Figure 5. The reference K0 sample shows a V_{OC} of 4.4 ± 0.6 V, which is shown as the red line. For non-porous graphene/PVDF nanofibers, the V_{OC} increases to 8.2 ± 1.1 V for the G0.1 sample and then drops to around 4 V for G1 and G3. Therefore, the optimum amount of graphene content for a solid core PVDF fiber is 0.1 wt%, which is in agreement with the previous report.[30]

The introduction of porosity enhances the V_{OC} value to 10.4 ± 1.2 V and 22.6 ± 3.1 V for B0 and S0 samples, respectively. Both porous fibers show larger V_{OC} than the K0 reference sample and the optimum non-porous graphene/PVDF G0.1 sample. For the B-series, the addition of only 0.1 wt% graphene enhances the V_{OC} further to 14.8 ± 2.1 V. However, further addition of graphene beyond 0.1 wt% reduces the V_{OC} of the B-series samples. In the case of the S-series samples, the porous fibers without graphene show remarkably large voltages of 22.6 ± 3.1 V. Adding graphene does not lead to further improvement of the voltage response and only deteriorates the performance of the pressure sensors. Generally, for non-porous or porous fibers (B-samples) fabricated in the binodal region, graphene content of just 0.1 wt% is the optimum value. Due to the conductive nature of graphene, it can be assumed that filler content above 0.1 wt% is above the percolation threshold. Thus, formation of a conductive path reduces the voltage response and is detrimental for the performance.[30] In case of S-samples, the percolation threshold is substantially
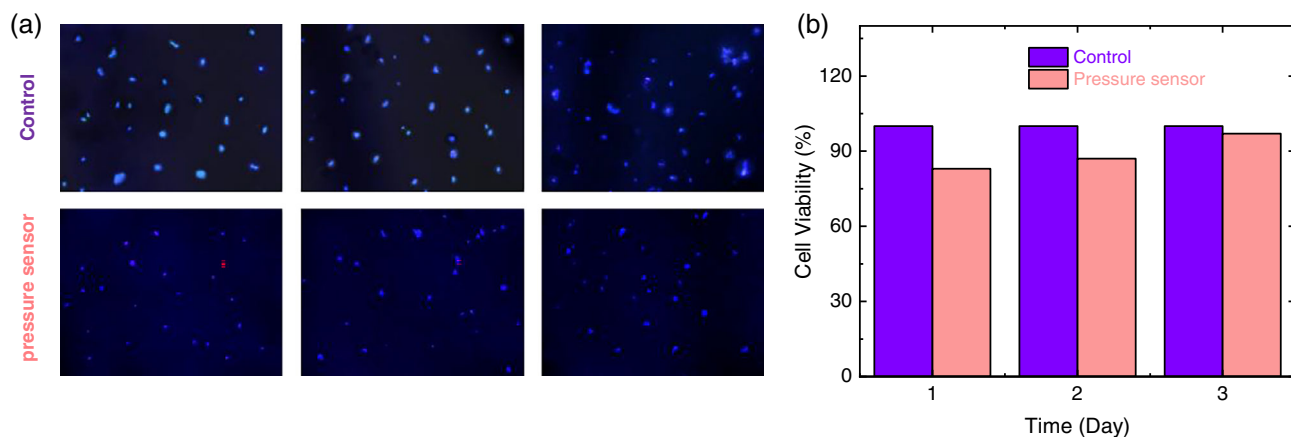
FIGURE 4 (a) Fluorescence images and (b) viability of MEF cells after being cultured on the cell culture dish (control) and a designed pressure sensor for 1, 2, and 3 days. MEF, mouse embryonic fibroblasts [Color figure can be viewed at wileyonlinelibrary.com]
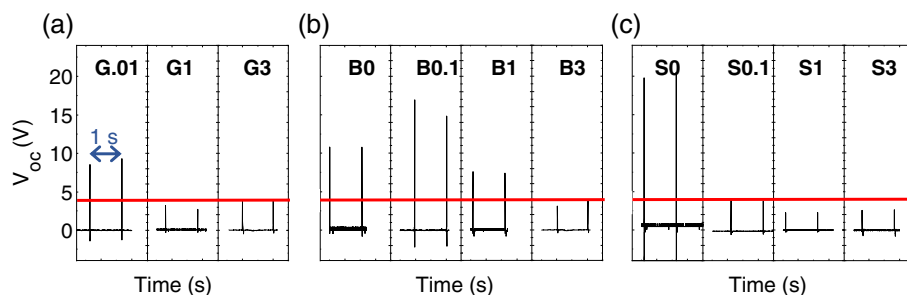
FIGURE 5 Measured V_{OC} of (a) PVDF-graphene nanofiber, (b) porous PVDF-graphene nanofiber prepared in the binodal region, and (c) porous PVDF-graphene nanofiber prepared in the spinodal region. The red line represents the K0 sample made of solid core PVDF nanofibers. All nanofiber layers experienced the same excitation with a mechanical force of 0.2 MPa. The cyclic response of the pressure sensors, V_{OC} and I_{SC}, are given at an impact frequency of 1 Hz. PVDF, poly(vinylidene fluoride) [Color figure can be viewed at wileyonlinelibrary.com]

lowered because of the increased porosity in the S-samples. Therefore, even 0.1 wt% of graphene in the nanocomposite is beyond the percolation threshold and decreases the response of the sensor.

The piezoelectric responses of PVDF fibers in G and S samples are proportional to β-phase content in PVDF fibers. G0.1 and S0 samples have shown highest output voltage and β-phase content among their related sample groups. However, addition of graphene has resulted in a decline in the piezoelectric response and β-phase content. Nonetheless in B samples, the piezoelectric output of PVDF fibers is not dependent on β-phase content. Non-porous PVDF fibers containing various amounts of graphene have shown the same amount of $F(\beta)$; however, the piezoelectric performance of sensor based on B0.1 sample is high, then it decreases to lower values for B1 and B3 samples. High-filler loadings might be above the percolation threshold of graphene and thus a conductive bridge is formed which leads to short-circuit in electrodes and a drop in piezoelectric output.[30]

Besides, the sensitivity parameter, S = V (open circuit voltage)/P (applied mechanical pressure), of B0.1 and S0 samples which has been calculated under a pressure of 0.2 MPa caused by mechanical impacting, amounts to values as high as 74 and 113 V/MPa, respectively.

Having established the optimal conditions for the nanofibers, the optimal sensors, based on B0.1 or S0 have been used for sensing the pressure of body movements. To prepare the sensor (Figure 6a), the sample with a size of 6×5 cm^2 has been sandwiched between two electrodes composed of Kapton tapes coated with aluminum (150 μm). The output performances of the sensor for the wrist and elbow bending are shown in Figure 6. The sensor generates large voltages as high as 1.5 ± 0.3 V for the wrist, and 2 ± 0.5 V for elbow movements. Furthermore, Figure S7 presents that the output voltage generated by the pressure sensor composed of B0.1 or S0 sample under walking is 4.96 ± 0.4 V. Such voltages are large enough that can be easily detected using simple wearable electronic circuits, which is designed for the pickup of
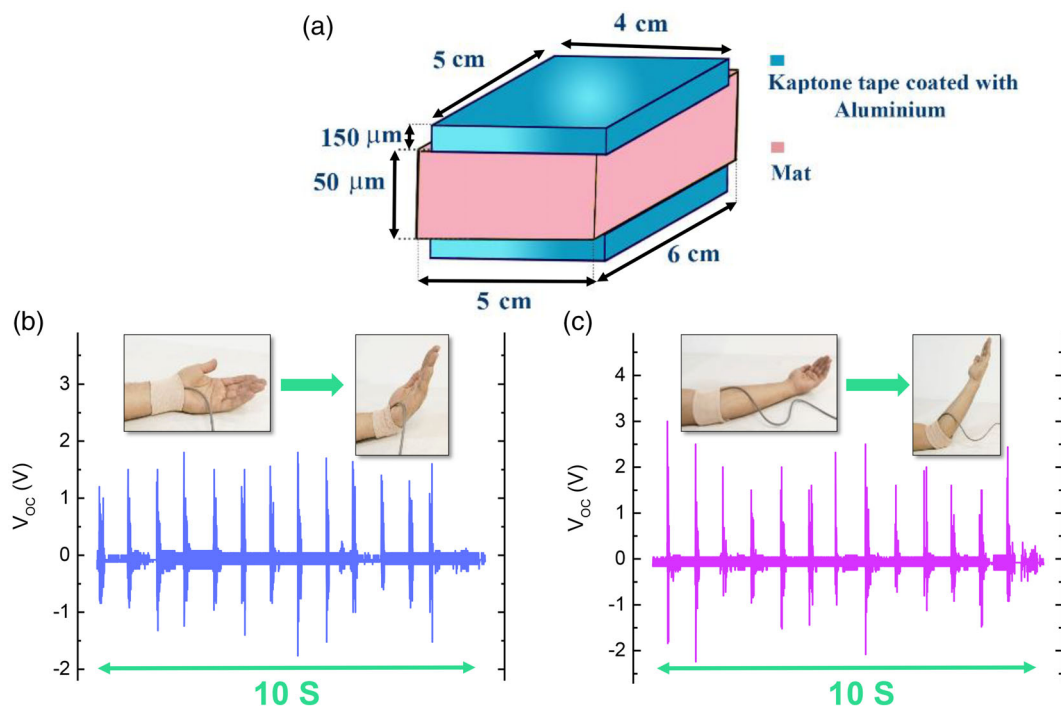
FIGURE 6 (a) Schematic of the pressure sensor. The output voltages of the pressure sensor under (b) wrist bending and (c) elbow bending [Color figure can be viewed at wileyonlinelibrary.com]

low-frequency signals.[54] The output of pressure sensor tested under cyclic pressure caused by finger tapping, presented in Figure S8, also suggests that the generated voltage by the sensor under cyclic pressing is constant at 0.47 ± 0.07 V, and does not change over time, guaranteeing stability and reproducibility of the sensor response. The results reveal that the outputs of the sensor are large enough that enable its application for pressure sensing of various body movements ranging from walking to subtle movements of arms and hands.

4 | CONCLUSION

In summary, a biocompatible and flexible piezoelectric pressure sensor has been demonstrated for movement monitoring. Four different nanofiber concepts, that is, pristine PVDF, graphene/PVDF composite, porous PVDF, and porous graphene/PVDF have been realized through a careful study of the ternary phase diagram of the PVDF/DMF (solvent)/water (non-solvent) system. It is shown that synergistic interaction between porosity and filler addition can only be achieved in nanofibers that are solidified in the binodal region of the phase diagram. The addition of just 0.1 wt% graphene is enough to enhance the voltage response of the fiber to 14.8 ± 2.1 V, which is a 3-fold increase in output voltage compared to that based on pristine PVDF fibers.

Graphene is a non-piezoelectric conductive filler. Hence, piezoelectric fillers can be suggested as a possible route to enhance further the voltage response of fibers that are solidified in the binary region of the phase diagram. However, this route may not be applicable for porous filler/PVDF nanofibers fabricated by driving the phase separation to the spinodal region, because as we demonstrated, the addition of graphene filler adversely affected the voltage response of the sensors. Therefore, a similar trend could be expected for other filler types.

The study of the PVDF/solvent/non-solvent phase diagram combined with solidification study of the ternary composite (PVDF/filler/pores) in the binodal or spinodal regions of the phase diagram can provide a good insight in optimizing and creating synergy between porosity and fillers to improve piezoelectric voltage response further for sensing applications.

DATA AVAILABILITY STATEMENT

No. Research data are not shared.

ORCID

Kamal Asadi 🅘 https://orcid.org/0000-0003-0447-4337

REFERENCES

[1] W. Guo, C. Tan, K. Shi, J. Li, X. X. Wang, B. Sun, X. Huang, Y. Z. Long, P. Jiang, _Nanoscale_ **2018**, _10_, 17751.

[2] S. Anwar, M. Hassanpour Amiri, S. Jiang, M. M. Abolhasani, P. R. F. Rocha, K. Asadi, _Adv. Funct. Mater._ **2021**, _31_, 2004326.

[3] H. Soleymani, M. Noormohammadi, M. A. Kashi, M. H. Amiri, J. J. Michels, K. Asadi, M. M. Abolhasani, _Adv. Mater. Interfaces_ **2021**, _8_, 2001734.

[4] M. M. Abolhasani, K. Shirvanimoghaddam, H. Khayyam, S. M. Moosavi, N. Zohdi, M. Naebe, _Polym. Test._ **2018**, _66_, 178.

[5] J. Chun, K. Y. Lee, C. Y. Kang, M. W. Kim, S. W. Kim, J. M. Baik, _Adv. Funct. Mater._ **2014**, _24_, 2038.

[6] S. Zhang, L. Zhang, L. Wang, F. Wang, G. Pan, _J. Mater. Chem. C_ **2019**, _7_, 4760.

[7] J. Yan, Y. Han, S. Xia, X. Wang, Y. Zhang, J. Yu, B. Ding, _Adv. Funct. Mater._ **2019**, _29_, 1907919.

[8] M. Baniasadi, J. Huang, Z. Xu, S. Moreno, X. Yang, J. Chang, M. A. Quevedo-Lopez, M. Naraghi, M. Minary-Jolandan, _ACS Appl. Mater. Interfaces_ **2015**, _7_, 5358.

[9] J. Fang, X. Wang, T. Lin, _J. Mater. Chem._ **2011**, _21_, 11088.

[10] Y.-L. Liu, Y. Li, J. T. Xu, Z. Q. Fan, _ACS Appl. Mater. Interfaces_ **2010**, _2_, 1759.

[11] M. M. Abolhasani, M. Naebe, Q. Guo, _J. Phys. Chem. Chem. Phys._ **2014**, _16_, 10679.

[12] M. Baqeri, M. M. Abolhasani, M. R. Mozdianfard, Q. Guo, A. Oroumei, M. Naebe, _J. Appl. Polym. Sci._ **2015**, _132_, 42304.

[13] Y. Xin, J. Zhu, H. Sun, Y. Xu, T. Liu, C. Qian, _Ferroelectrics_ **2018**, _526_, 140.

[14] G. Kalimuldina, N. Turdakyn, I. Abay, A. Medeubayev, A. Nurpeissova, D. Adair, Z. Bakenov, _Sensors_ **2020**, _20_, 5214.

[15] Y. Yang, A. Centrone, L. Chen, F. Simeon, T. Alan Hatton, G. C. Rutledge, _Carbon_ **2011**, _49_, 3395.

[16] C.-T. Pan, C. C. Chang, Y. S. Yang, C. K. Yen, Y. H. Kao, Y. L. Shiue, _Sens. Actuators, A_ **2020**, _301_, 111708.

[17] H. Khan, A. Razmjou, M. Ebrahimi Warkiani, A. Kottapalli, M. Asadnia, _Sensors_ **2018**, _18_, 418.

[18] S. Garain, S. Jana, T. K. Sinha, D. Mandal, _ACS Appl. Mater. Interfaces_ **2016**, _8_, 4532.

[19] X. Yang, Y. Wang, X. Qing, _Sens. Actuators, A_ **2019**, _299_, 111579.

[20] H. Yu, T. Huang, M. Lu, M. Mao, Q. Zhang, H. Wang, _Nanotechnology_ **2013**, _24_, 405401.

[21] R. K. Singh, S. W. Lye, J. Miao, _Sens. Actuators, A_ **2020**, _303_, 111841.

[22] C. Sun, J. Zhang, Y. Zhang, F. Zhao, J. Xie, Z. Liu, J. Zhuang, N. Zhang, W. Ren, Z. G. Ye, _Appl. Surf. Sci._ **2021**, _562_, 150126.

[23] A. Chinnappan, C. Baskar, S. Baskar, G. Ratheesh, S. Ramakrishna, _J. Mater. Chem. C_ **2017**, _5_, 12657.

[24] H. Fashandi, M. M. Abolhasani, P. Sandoghdar, N. Zohdi, Q. Li, M. Naebe, _Cellulose_ **2016**, _23_, 3625.

[25] D. Mandal, K. Henkel, D. Schmeißer, _J. Phys. Chem. Chem. Phys._ **2014**, _16_, 10403.

[26] F. Mokhtari, M. Shamshirsaz, M. Latifi, S. Asadi, _J. Text. Inst._ **2016**, _108_, 906.

[27] S. Azimi, A. Golabchi, A. Nekookar, S. Rabbani, M. H. Amiri, K. Asadi, M. M. Abolhasani, _Nano Energy_ **2021**, _83_, 105781.

[28] A. Samadi, R. Ahmadi, S. M. Hosseini, _Org. Electron._ **2019**, _75_, 105405.

[29] A. Samadi, S. Pourahmad, _Int. J. Energy Res._ **2020**, _44_, 10087.

[30] M. M. Abolhasani, K. Shirvanimoghaddam, M. Naebe, _Compos. Sci. Technol._ **2017**, _138_, 49.

[31] R. Richert, _Eur. Phys. J. Spec. Top._ **2010**, _189_, 37.

[32] F. Kremer, A. Schönhals, _Broadband Dielectric Spectroscopy_, Springer, New York City **2003**, p. 99.

[33] K. W. Wagner, _Electr. Eng. (Archiv fur Elektrotechnik)_ **1914**, _2_, 371.

[34] R. Sillars, _J. Inst. Electr. Eng._ **1937**, _80_, 378.

[35] M. M. Abolhasani, M. Naebe, K. Shirvanimoghaddam, H. Fashandi, H. Khayyam, M. Joordens, A. Pipertzis, S. Anwar, R. Berger, G. Floudas, J. Michels, K. Asadi, _Nano Energy_ **2019**, _62_, 594.

[36] M. M. Abolhasani, M. Naebe, M. Hassanpour Amiri, K. Shirvanimoghaddam, S. Anwar, J. J. Michels, K. Asadi, _Adv. Sci._ **2020**, _7_, 2000517.

[37] Y.-S. Kim, Y. Xie, X. Wen, S. Wang, S. J. Kim, H. K. Song, Z. L. Wang, _Nano Energy_ **2015**, _14_, 77.

[38] H. Fashandi, A. Yegane, M. M. Abolhasani, _Fibers Polym._ **2015**, _16_, 326.

[39] J. Mulder, _Basic Principles of Membrane Technology_, Springer Science & Business Media, Berlin **2012**.

[40] H. Matsuyama, M. Teramoto, R. Nakatani, T. Maki, _J. Appl. Polym. Sci._ **1999**, _74_, 159.

[41] M. Karimi, W. Albrecht, M. Heuchel, M.H. Kish, J. Frahn, Th. Weigel, D. Hofmann, H. Modarress, A. Lendlein, _J. Membr. Sci._ **2005**, _265_, 1.

[42] F. W. Altena, C. Smolders, _Macromolecules_ **1982**, _15_, 1491.

[43] J. Zheng, H. Zhang, Z. Zhao, C. C. Han, _Polymer_ **2012**, _53_, 546.

[44] Y.-A. Seo, H. R. Pant, R. Nirmala, J. H. Lee, K. G. Song, H. Y. Kim, _J. Porous Mater._ **2012**, _19_, 217.

[45] A. Salimi, A. Yousefi, _J. Polym. Sci. Part B: Polym. Phys._ **2004**, _42_, 3487.

[46] J. Andrew, D. Clarke, _Langmuir_ **2008**, _24_, 8435.

[47] S. Huang, W. A. Yee, W. C. Tjiu, Y. Liu, M. Kotaki, Y. C. F. Boey, J. Ma, T. Liu, X. Lu, _Langmuir_ **2008**, _24_, 13621.

[48] L. Yu, P. Cebe, _Polymer_ **2009**, _50_, 2133.

[49] S. K. Karan, R. Bera, S. Paria, A. K. Das, S. Maiti, A. Maitra, B. B. Khatua, _Adv. Energy Mater._ **2016**, _6_, 1601016.

[50] M. A. Rahman, G.-S. Chung, _J. Alloys Compd._ **2013**, _581_, 724.

[51] N. L. Meereboer, I. Terzić, S. Saidi, D. Hermida Merino, K. Loos, _ACS Macro Lett._ **2018**, _7_, 863.

[52] W. A. Yee, M. Kotaki, Y. Liu, X. Lu, *Polymer* **2007**, *48*, 512.

[53] M. M. Abolhasani et al., *Nano* **2014**, *9*, 1450065.

[54] X. Wang, P. R. Wilson, R. B. Leite, G. Chen, H. Freitas, K. Asadi, E. C. P. Smits, I. Katsouras, P. R. F. Rocha, *Energy Technol.* **2020**, *8*, 2000114.

SUPPORTING INFORMATION

Additional supporting information may be found in the online version of the article at the publisher's website.